Front. Environ. Sci. Eng. 2024, 18(2): 19
https://doi.org/10.1007/s11783-024-1779-4

RESEARCH ARTICLE

A potential threat from biodegradable microplastics: mechanism of cadmium adsorption and desorption in the simulated gastrointestinal environment

Timing Jiang[1,3], Xiang Wu (✉)[1,2], Shushan Yuan (✉)[1,3], Changfei Lai[1,3], Shijie Bian[1,3], Wenbo Yu[1,3], Sha Liang[1,3], Jingping Hu[1,3], Liang Huang[1,3], Huabo Duan[1,3], Yafei Shi[4], Jiakuan Yang[1,3,5]

1 School of Environmental Science & Engineering, Huazhong University of Science and Technology, Wuhan 430074, China
2 School of Resources and Environmental Science, Hubei University, Wuhan 430062, China
3 Hubei Provincial Engineering Laboratory for Solid Waste Treatment Disposal and Recycling, Wuhan 430074, China
4 School of Civil Engineering, Architecture and Environment, Hubei University of Technology, Wuhan 430068, China
5 State Key Laboratory of Coal Combustion, Huazhong University of Science and Technology, Wuhan 430074, China

HIGHLIGHTS

- The Cd(II) adsorption capacity followed the order of PA > PLA > PP.
- Oxygen groups played critical roles in Cd(II) adsorption by PLA MPs.
- Degradation of PLA MPs enhanced Cd(II) desorption in human digestive fluid.
- Cd(II) release was easier from PLA during human digestion than from PP or PA.

ARTICLE INFO

Article history:
Received 3 April 2023
Revised 21 August 2023
Accepted 23 August 2023
Available online 25 September 2023

Keywords:
Biodegradable microplastics
Cadmium
Adsorption and desorption
Gastrointestinal environment
Two-dimensional correlation spectroscopy
Bioaccessibility

GRAPHIC ABSTRACT

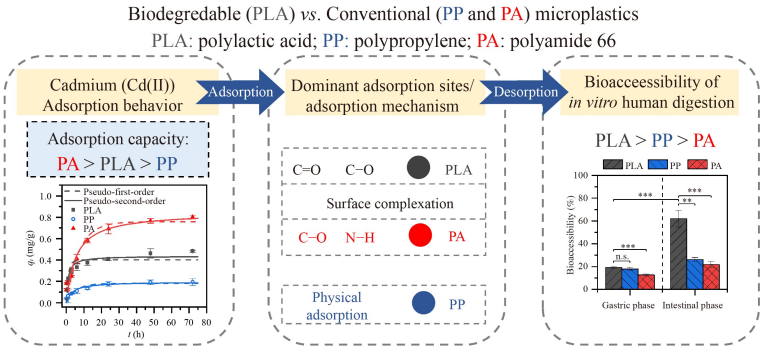

ABSTRACT

It has been demonstrated that microplastics (MPs) can accumulate heavy metals from the environment and transfer them into organisms via the food chain. However, adsorption and desorption capacities for biodegradable MPs relative to those for conventional MPs remain poorly understood. In this study, cadmium (Cd(II)) adsorption and desorption characteristics of polylactic acid (PLA), a typical biodegradable MP, were investigated. Two conventional MPs, i.e., polypropylene (PP) and polyamide (PA) were used for comparison. The maximum Cd(II) adsorption capacities of the MPs studied in the adsorption experiments decreased in the order PA (0.96 ± 0.07 mg/g) > PLA (0.64 ± 0.04 mg/g) > PP (0.22 ± 0.03 mg/g). The Pseudo-second-order kinetic model and Freundlich isothermal model described the Cd(II) adsorption behaviors of PLA MPs well. X-ray photoelectron spectroscopy and two-dimensional Fourier transform infrared correlation spectroscopy analysis indicated that oxygen functional groups were the major and preferential binding sites of PLA MPs, which contributed to their high Cd(II) adsorption capacities. Simulated gastric and intestinal fluids both significantly enhanced the desorption capacities of the examined MPs. Notably, degradation of the PLA MPs during *in vitro* human digestion made the Cd(II) on the PLA MPs more bioaccessible (19% in the gastric phase and 62% in the intestinal phase) than Cd(II) on the PP and PA MPs. These results indicate the remarkable capacities of biodegradable MPs to accumulate Cd(II) and transfer it to the digestive system and show that biodegradable MPs might pose more severe threats to human health than conventional nonbiodegradable MPs.

1 Introduction

Global plastics production exceeded 360 million tons in

✉ Corresponding authors
E-mails: xiangwu@hubu.edu.cn (X. Wu); yuanss@hust.edu.cn (S. Yuan)

2020, most of which was petroleum-based and nonbiodegradable (Plastics Europe, 2021). The increasing consumption of plastic products and associated waste mismanagement practices have led to substantial amounts of plastics litter and microplastics (MPs), resulting in their ubiquitous distribution in the global environment (UNEP, 2021). With the growing public awareness of plastic and MP pollution, biodegradable plastics have been presented as promising alternatives to conventional plastics (i.e., petroleum-based plastics). Polylactic acid (PLA), for example, is the most representative biodegradable polymer, and it accounts for more than 20% of the total global production of biodegradable plastics (Haider et al., 2019). Plastics labeled biodegradable are generally thought to degrade completely into water, carbon dioxide, and biomass. However, the degradation processes of biodegradable plastic such as PLA are initiated by suitable conditions, including heat, moisture, and specific enzymes, and might be very slow or even fail to occur for years under natural environmental conditions, as previously reported (Napper and Thompson, 2019). Thus, biodegradable plastics irrevocably undergo fragmentation into MPs in much the same way as conventional plastics do (Wei et al., 2021). Although the global environmental distribution of biodegradable MPs is uncertain so far, their negative ecological effects could be comparable to those of conventional MPs, as indicated with a range of terrestrial and aquatic organisms (Liu and Wang, 2020; Duan et al., 2022).

The negative impacts of MPs may be manifested by not only their inherent toxicity but also the combined toxic effects with other coexisting contaminants, including heavy metals (Prata et al., 2020). Heavy metals are among of the most critical contaminants due to their high toxicities, mobilities, and bioaccumulation capacities, and available evidence has indicated that MPs can accumulate heavy metal ions from the surrounding environment (Sarkar et al., 2021). Moreover, MPs can serve as effective vectors to transfer the adsorbed heavy metals into organisms, including humans, via the food chain, leading to subsequent toxic effects (Oliveri Conti et al., 2020).

Adsorption is the key environmental process of the interactions between MPs and coexisting contaminants. A growing number of investigations have provided critical insights into the heavy metals adsorption characteristics and mechanisms of various polymer MPs (Dong et al., 2019; Tang et al., 2020). Specifically, most of the previous investigators focused on polypropylene (PP), polyethylene (PE), and polystyrene (PS) MPs, since these polymers have the largest consumption rates of plastic products and generate the most widely distributed MP contaminants in the environment. As reported, they account for over 60% of all MPs detected in freshwater (Li et al., 2020). In many cases, it has been demonstrated that physical adsorption dominates the interactions between heavy metals and the abovementioned MPs and that their adsorption capacities are highly contingent on the physical characteristics, including surface area, pore volume, particle size, and crystallinity (Wang et al., 2019; Zhou et al., 2020). Moreover, a few other studies reported remarkably higher adsorption capacities on the MPs of other polymers, especially polyamide (PA) and polymethyl methacrylate (PMMA), which warrant further investigation due to their higher potential risks. For instance, Li et al. (2019) demonstrated that PA MPs exhibited the largest cadmium (Cd(II)) adsorption affinity among the examined MPs (polyvinyl chloride (PVC), PP, PE, and PS), and this was supported by Zhou et al. (2020). Yang et al. (2019) observed that the copper (Cu(II)) adsorption capacities of PA and PMMA MPs were over 30 and 4 times higher, respectively, than those of PE, PS, and other examined MPs, which is probably related to their specific polar groups (–NHCO– and –COO–). Tang et al. (2021) proved that surface complexation was the dominant adsorption mechanism of nylon MPs. The above studies indicated that the adsorption mechanisms were complicated and varied among MPs from different polymers and led to different adsorption abilities.

In addition, since MPs can enter the human body through oral intake, the ecological risks of heavy metals adsorbed on MPs largely depend on desorption in the human digestive system. Furthermore, previous studies have shown that heavy metals on MPs are more easily released *in vivo* (e.g., in the digestive system) than in freshwater and soil, as the complicated bioecological conditions in gastrointestinal fluids can enhance their desorption (Liao and Yang, 2020; Li et al., 2022). This is known as bioaccessibility (defined as the proportion of heavy metals desorbed from the sorbent in the digestive system), which is commonly evaluated by performing standardized in vitro assays that mimic human digestion (Ruby et al., 1996; Liao and Yang, 2022). However, most of the previous literature was focused solely on the adsorption and desorption behaviors of conventional nonbiodegradable MPs, and it remains unclear whether biodegradable MPs have comparable adsorption and desorption capacities.

In the current study, Cd(II) was selected as the target heavy metal contaminant, and PLA was selected as a representative biodegradable MP for comparison with two conventional MPs of similar particle sizes, namely, PP and PA. The primary objectives of the current study were to 1) compare the Cd(II) adsorption behaviors and mechanisms of biodegradable PLA MPs with those of conventional nonbiodegradable MPs; 2) assess the desorption capabilities and bioaccessibilities of Cd(II) adsorbed on PLA MPs in an *in vitro* human gastrointestinal environment in comparison with those of conventional nonbiodegradable MPs. A schematic for this study is presented in Fig. S1.

2 Materials and methods

2.1 Raw materials and reagents

The biodegradable PLA MPs used in the current study were obtained from Zhongcheng Plastic Co. Ltd. (Dongguan, China). PP and PA (polyamide 66) were acquired from Jiecheng Plastic Chemical Co. Ltd. (Dongguan, China) as representatives of conventional nonbiodegradable plastics. These MP particles with irregular shapes were passed through sieves, and MPs with sizes of 100–200 μm were collected for experiments and characterization. Before they were used in the adsorption and characterization experiments, the MPs were washed three times with ultrapure water and dried at room temperature.

Pepsin (porcine, 1:15000), pancreatin (porcine, USP), lipase (porcine, 15–35 units/mg), and *l*-lactic acid (≥ 98%(T)) were acquired from Aladdin Chemical Reagent Co. Ltd. (Shanghai, China). Bile salts (biotechnology grade) were acquired from Macklin Biochemical Co. Ltd. (Shanghai, China). Lactic acid detection kits were acquired from Jiancheng Biotechnology Co. Ltd. (Nanjing, China). Other reagents (such as $Cd(NO_3)_2 \cdot 4H_2O$, $NaNO_3$, etc.) were all acquired from Sinopharm Chemical Reagent Co. Ltd. (Shanghai, China) and were of analytical reagent grade.

Before use, all glass vessels were soaked in 10% (v/v) HNO_3 for over 12 h, rinsed thoroughly with ultrapure water, and then dried. The Cd(II) solution used in adsorption experiments was prepared with $Cd(NO_3)_2$ and a background $NaNO_3$ solution (0.01 mol/L, pH = 6.00 ± 0.02).

2.2 Adsorption batch experiments

The adsorption experiments were conducted in clear glass vials with Teflonlined screw caps (CNW Technologies GmbH, Germany), and 200 mg MP samples with 20 mL of the Cd(II) solution were added to each. For the adsorption kinetic experiments, the initial Cd(II) concentration was set to 100 mg/L. Each vial was placed in an incubator shaker for constant horizontal shaking in the dark (150 r/min, 25 °C). After the designated time periods (0.25, 0.5, 1, 3, 6, 12, 24, 48, and 72 h), the samples were passed through a 0.45 μm filter and then the Cd(II) concentrations were measured via flame atomic absorption spectrometry (FAAS, novAA 400P, Germany). The filtered MP samples were collected and dried at room temperature and then prepared for desorption experiments and FTIR analyses.

For the adsorption isotherm experiments, a series of Cd(II) solution were prepared with concentrations of 10, 20, 40, 60, 80, 100, 120, 160, and 200 mg/L. After shaking for 72 h, the solutions were filtered and then subjected to Cd(II) measurement via FAAS. The filtered MP samples with initial concentrations of 200 mg/L were collected and dried at room temperature and prepared for XPS analyses.

The adsorption capacities of the MPs (mg/g) were calculated as follows (Eq. (1)):

$$q_t = \frac{(C_0 - C_t)V}{m}, \quad (1)$$

where C_0 and C_t are the initial and remaining Cd(II) concentrations of the filtered solution (mg/L), respectively; V is the volume of the solution (L); and m is the mass of MPs (g). All experiments were conducted in triplicate with the mean values reported.

2.3 *In vitro* desorption experiments

The physiologically based extraction test (PBET), an *in vitro* assay, was utilized to assess the desorption and bioaccessibility of Cd(II) absorbed on MPs in human gastric and intestinal phases (Ruby et al., 1996). MP samples with adsorbed Cd(II) were collected after the adsorption kinetics experiments and then dried at room temperature. The simulated gastric fluid and intestinal fluid for human digestion based on the PBET were prepared within 12 h prior to use. Briefly, the composition of 1 L of the gastric fluid (pH = 2.5) included sodium malate (0.50 g), tri-sodium citrate (0.50 g), lactic acid (420 μL), glacial acetic acid (500 μL), and pepsin (1.25 g). The composition of 1 L of the intestinal fluid (pH = 7.0) consisted of bile salts (1.78 g), pancreatin (0.5 g), and lipase (1.6 g).

To model the gastric phase, 100 mg MP samples were mixed in vials with 10 mL of gastric fluid and shaken for 1 h (150 r/min, 37 °C); then, for the intestinal phase, the gastric phase mixture was adjusted to a pH of 7.0 using saturated Na_2CO_3 solution, 10 mL of intestinal fluid was added, and the mixture was shaken for 5 h (150 r/min, 37 °C). After each phase, the mixture was filtered, followed by Cd(II) measurement and lactic acid detection. The MP samples were collected, washed with 1% sodium dodecyl sulfate solution, ethanol, and ultrapure water, and then dried. Additionally, two control groups (referred to as Ctrl (1 h) and Ctrl (5 h)) were used to represent the aquatic environment, and the gastric and intestinal fluid was replaced with the $NaNO_3$ background solution (25 °C) used in the adsorption experiments. The blank control group (Blank) was prepared without MPs.

The desorption capacities of the MPs (mg/g) were calculated as follows (Eq. (2)):

$$q_d = \frac{C_e^d V}{m}, \quad (2)$$

where C_e^d is the Cd(II) concentration of the filtered solution after desorption (mg/L).

The bioaccessibilities of Cd(II) on the MPs in the gastric and intestinal phases were calculated as follows (Eq. (3)):

$$\text{Bioaccessiblity}(\%) = \frac{\text{Cd(II) desorbed } \textit{in vitro}}{\text{Cd(II) adsorbed on MPs}} \times 100\% = \frac{q_d}{q_e} \times 100\%, \quad (3)$$

where q_e is the Cd(II) concentration on the MPs at adsorption equilibrium (mg/g).

2.4 Data and statistical analyses

All adsorption and desorption experiments were conducted in triplicate, and the mean values were reported. The Pseudo-first-order kinetic model, Pseudo-second-order kinetic model, film diffusion model, and intraparticle diffusion model were utilized to study the Cd(II) adsorption behaviors of the three examined MPs. The Langmuir model, Freundlich model, and Dubbin-Radushkevich model were used to fit the adsorption isotherms. These model expressions are shown in Text S1.

Pearson correlation analyses were performed with SPSS Statistics (SPSS 18.0, IBM, USA), and the differences were determined through one-way analysis of variance (ANOVA) with replication (n = 3) and were considered significant when the p-value was below 0.05.

2.5 MP characterization

Scanning electron microscopy (SEM, GeminiSEM 300, ZEISS, Germany) was used to investigate the morphologies of the MP samples before and after adsorption, as well as after desorption in the gastric and intestinal phases. An N_2 adsorption-desorption analytical method was adopted to determine the Brunauer–Emmett–Teller (BET) specific surface area and total pore volume. The crystalline structure of the original MP samples as well as crystallinity was studied with X-ray diffraction (XRD, XRD-7000, Shimadzu, Japan) over the 2θ range 10°–80°.

To determine the surface chemical compositions of the MPs, both the MPs samples before and after Cd(II) adsorption were analyzed by X-ray photoelectron spectroscopy (XPS) and Fourier transform infrared spectroscopy (FTIR). The XPS spectra and elemental abundance information were obtained with an X-ray spectrometer (K-Alpha, Thermo Fisher Scientific Inc., USA). The FTIR spectra were obtained in the region of 4000–400 cm^{-1} with a Nicolet FT-IR spectrometer (iS50R, Thermo Fisher Scientific Inc., USA) operated in the attenuated total reflectance mode.

To further interpret the sequential changes in the FTIR spectra during Cd(II) adsorption kinetics of the three examined MPs, perturbation-based generalized two-dimensional FTIR correlation spectroscopy (2D FTIR COS) analysis was applied. The adsorption time (0–72 h) was used as an external perturbation variable. The FTIR data sets were normalized with the summed absorbance of 4000–400 cm^{-1}. Then, 2D FTIR COS maps were plotted with download-free 2DShige software. The synchronous and asynchronous 2D FTIR correlation spectra were interpreted according to Noda's rules (Noda and Ozaki, 2005).

3 Results and discussion

3.1 Basic characteristics of the MPs

Irregular shapes with cracks, wrinkles, and pits were observed in the SEM images of the three original MPs (Fig. 1). Compared to the PP and PA MPs, the PLA MPs showed rougher surfaces and more wrinkles, which suggested a higher surface area. As listed in Table S1, the specific surface area decreased in the order PLA (4.90 m^2/g) > PP (4.16 m^2/g) > PA (3.18 m^2/g), which was consistent with their surface morphologies. The values of micropore volume (< 2 nm) were below the detection limit (< 0.00001 cm^3/g), and the volume of 2–10 nm exhibited the largest proportion (59.96%–69.34%) of the pore volume. The crystallinities according to the XRD patterns (Fig. S2) were 40.85%, 30.99%, and 27.46% for the PLA, PP, and PA MPs, respectively.

3.2 Adsorption behaviors of Cd(II) on the MPs

3.2.1 Adsorption kinetics

The kinetic data for Cd(II) adsorption on the PLA, PP, and PA MPs are shown in Fig. 2(a), together with the fits obtained with the Pseudo-first-order and Pseudo-second-order kinetic models. For all three MPs, dynamic equilibrium was almost achieved within approximately 48 h, and obvious distinctions in the equilibrium adsorption capacities (q_e) were observed. The q_e values determined with the Pseudo-second-order model decreased in the order PA (0.85 ± 0.06 mg/g) > PLA (0.44 ± 0.02 mg/g) > PP (0.20 ± 0.01 mg/g) (Table 1). Based on the correlation coefficient (R^2), the Pseudo-second-order model gave better fits to the kinetic data for these three MPs than the Pseudo-first-order model, implying a combination of multiple adsorption processes (Guo et al., 2020; Tang et al., 2020).

To confirm the rate-limiting step during the adsorption process, both the film diffusion and intraparticle diffusion models were evaluated. As shown in the Boyd plots (Fig. 2(b)), the curve for all three MPs gave linear fits (Table S2) that did not pass through the origin, suggesting the involvement of film diffusion (Qiu et al., 2019). The fitting results of the intraparticle diffusion model were multilinear during the entire time (Fig. 2(c)), indicating that the adsorption process was influenced by at least two critical steps (Guo et al., 2020). The multilinear fitting plot was subdivided to interpret the Cd(II) adsorption process. In the first stage (0–1 h), the Cd(II) in solution

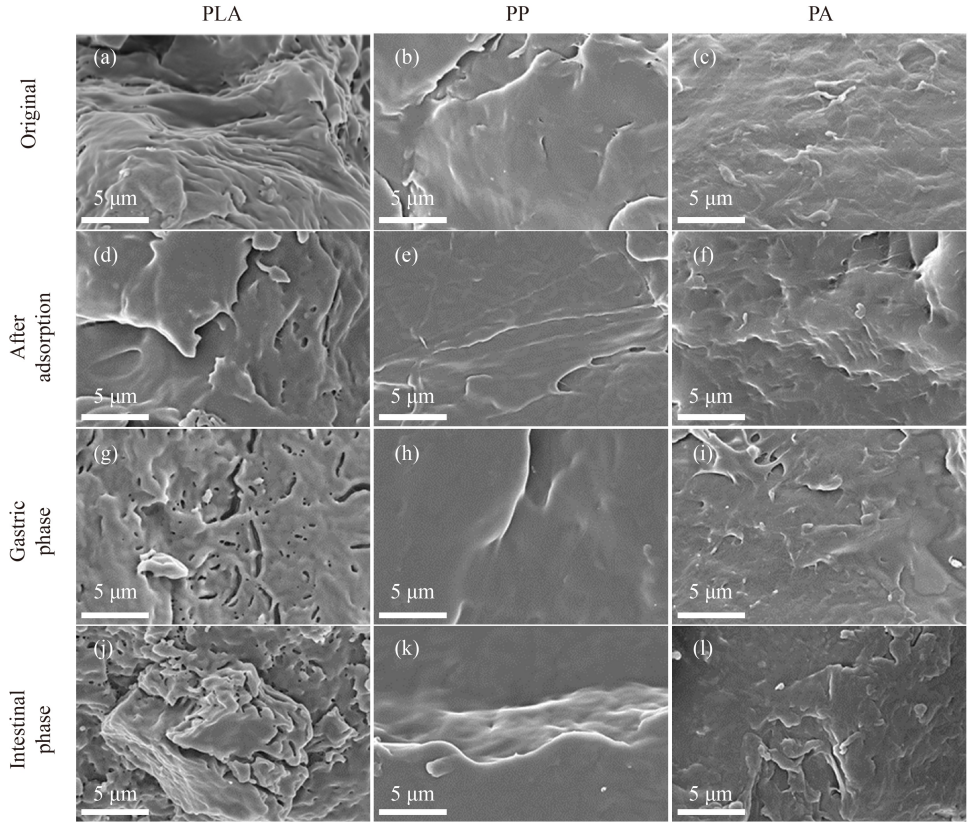

Fig. 1 SEM images of PLA, PP, and PA microplastics (MPs) on a scale of 5 μm: original MPs (a, b, c), MPs after adsorption (d, e, f), MPs in the gastric phase (g, h, i), and MPs in the intestinal phase (j, k, l).

Table 1 Fitting parameters of kinetic models for adsorption of Cd(II) on PLA, PP, and PA microplastics (MPs) (the Cd(II) concentration = 100 mg/L, and the MP dose = 10 g/L)

Kinetic model	Parameters	PLA	PP	PA
Pseudo-first-order	k_1 (h^{-1})	0.84 ± 0.27	0.19 ± 0.05	0.14 ± 0.03
	q_e (mg/g)	0.40 ± 0.03	0.18 ± 0.01	0.76 ± 0.05
	R^2	0.763	0.861	0.916
Pseudo-second-order	k_2 (g/(mg·h))	2.35 ± 0.67	1.50 ± 0.48	0.22 ± 0.07
	q_e (mg/g)	0.44 ± 0.02	0.20 ± 0.01	0.85 ± 0.06
	R^2	0.903	0.929	0.943

diffused rapidly to the exterior surfaces of the MPs through liquid film diffusion. In the next stage (1–24 h), the adsorption process slowed gradually, and particle diffusion into the internal pores became dominant. Finally, in the third stage (> 24 h), adsorption quasi equilibrium was achieved. Notably, PLA MPs showed a higher adsorption rate (k_{p1} = 0.21 mg/(g·$h^{0.5}$)) than PP and PA MPs (k_{p1} = 0.06 and 0.15 mg/(g·$h^{0.5}$)) in the first stage (Table S3), probably due to the high specific surface areas of the PLA MPs (4.90 m^2/g). Then, the adsorption rate of PLA MPs (k_{p2} = 0.04 mg/(g·$h^{0.5}$)) dropped quickly, and the process became slower than that of PA MPs (k_{p2} = 0.14 mg/(g·$h^{0.5}$)). Additionally, PP MPs showed the slowest rate together with the lowest adsorption capacity during the whole process. In general, the adsorption kinetics indicated that the Cd(II) adsorption on the MPs was a multiple-step procedure in which both liquid film and intraparticle diffusion were involved.

3.2.2 Adsorption isotherms

In the adsorption isotherm experiments, the detected maximum adsorption capacities of these three MPs decreased in the order PA (0.96 ± 0.07 mg/g) > PLA (0.64 ± 0.04 mg/g) > PP (0.22 ± 0.03 mg/g), as shown in Fig. 3(a). The Langmuir and Freundlich fits to the data for the PLA, PP, and PA MPs are demonstrated in Figs. 3(b) and 3(c), respectively. Additionally, the parameters for the Langmuir, Freundlich, and Dubbin-

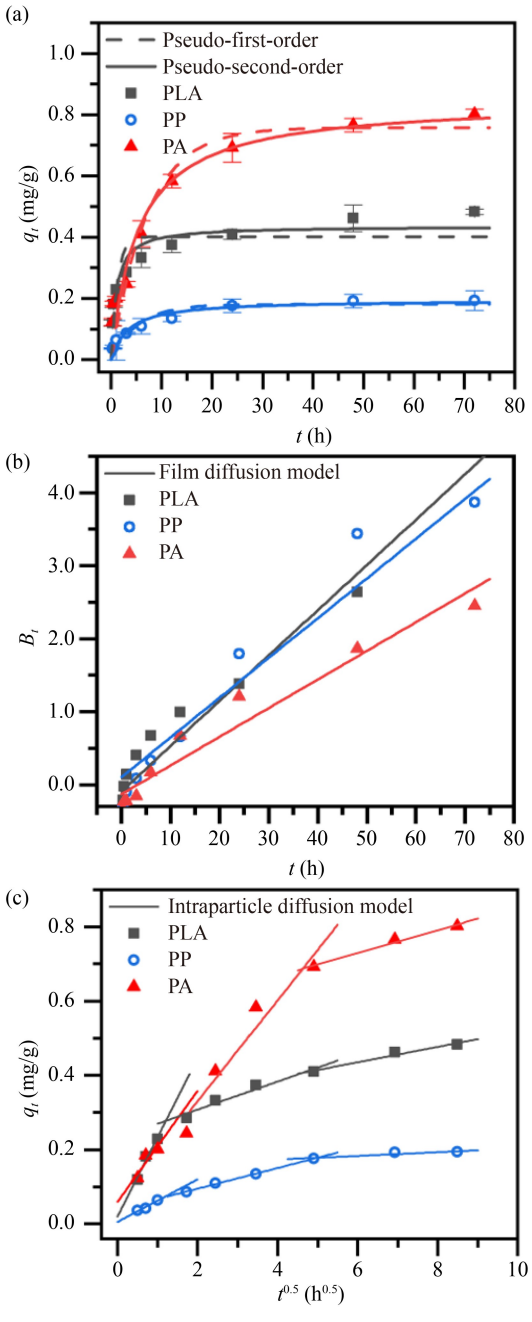

Fig. 2 Kinetics for adsorption of Cd(II) on PLA, PP, and PA microplastics (MPs) and fits with the (a) Pseudo-first-order and Pseudo-second-order models, (b) film diffusion model, and (c) intra-particle diffusion model.

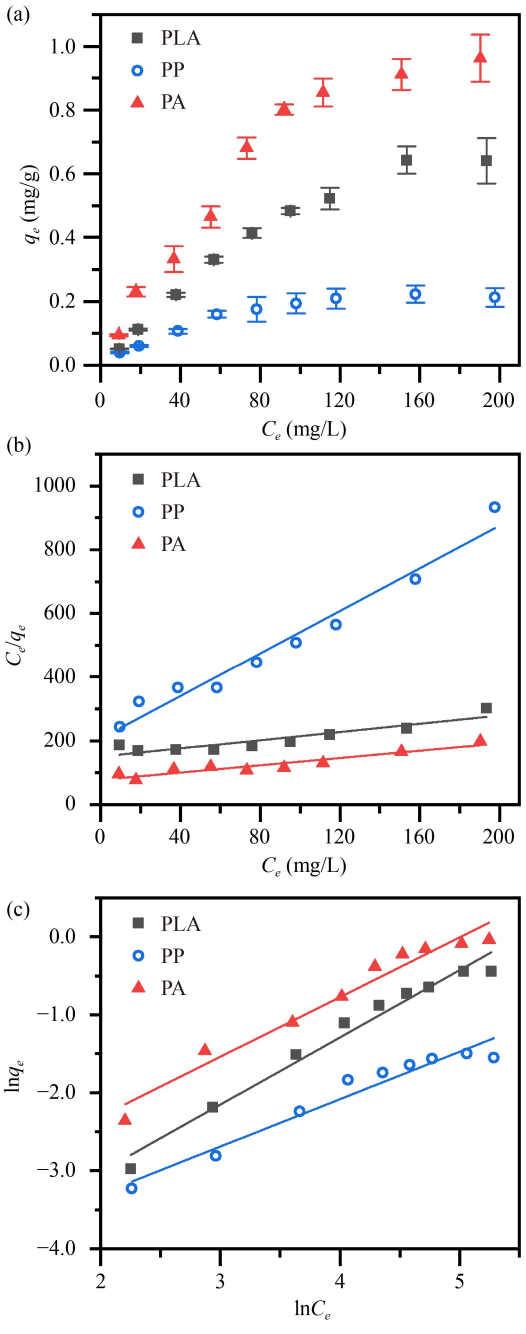

Fig. 3 Isotherms for adsorption of Cd(II) on PLA, PP, and PA microplastics (MPs): (a) original data, (b) Langmuir model, and (c) Freundlich model.

Radushkevich models are provided in Table 2. The R^2 values demonstrated that the adsorption isotherms for both the PLA and PA MPs were more precisely described by the Freundlich model than by the Langmuir and Dubbin-Radushkevich models. Both the Freundlich and Langmuir models provided good fits to the isothermal data for the PP MPs. Additionally, the n values of the Freundlich model (Table 2) with the three MPs decreased in the order PP > PA > PLA. The lowest n value for the PLA MPs suggested a heterogeneous distribution of adsorption sites, possibly attributable to specific interactions (Zhang et al., 2018).

3.3 Surface chemical changes of the MPs

3.3.1 XPS spectra of the MPs before and after Cd(II) adsorption

The element compositions of these three MPs were

Table 2 Fitting parameters of Isotherm models for Cd(II) adsorption on PLA, PP, and PA microplastics (MPs) (Cd(II) concentration = 10–200 mg/L, and equilibrium time = 72 h)

Isotherm model	Parameters	PLA	PP	PA
Langmuir	q_m (mg/g)	1.65 ± 0.30	0.34 ± 0.03	1.76 ± 0.24
	k_L (L/mg)	0.0042 ± 0.0011	0.0126±0.0030	0.0079±0.0019
	R^2	0.811	0.927	0.887
Freundlich	k_F (mg/g)	0.0087 ± 0.0018	0.0091 ± 0.0022	0.0223 ± 0.0057
	n	1.16 ± 0.07	1.56 ± 0.14	1.31 ± 0.11
	R^2	0.976	0.946	0.956
Dubbin-Radushkevich	k_{DR} (kJ/mol)	27.6 ± 6.4	38.8 ± 8.0	32.4 ± 6.3
	R^2	0.718	0.763	0.785

determined with XPS before and after Cd(II) adsorption, and their results are listed in Table 3. After adsorption, the atomic percentage of O 1s and the O/C ratio increased in both PLA and PP MPs. For the PA MPs after Cd(II) adsorption, the atomic percentage of N 1s and the N/C ratio increased by 2.89% and 0.04, respectively, and the O 1s and the O/C ratio decreased. No obvious Cd 3d peaks were detected for the three MPs after Cd(II) adsorption, possibly due to the small quantities of Cd(II) ions adsorbed on the surfaces of the MPs (< 1 mg/g as listed in Fig. 3(a)). The C 1s spectrum of PLA (Fig. 4(a) and Table 4) showed typical binding energies for C–C/C–H (284.77 eV), **C**–O–C=O (286.68 eV), and O=C–O (288.77 eV) groups, consistent with the results of Yu et al. (2023). The significant increment, as well as peak shifts for both C–O–C=O (from 286.68 eV: 23.00% to 286.73 eV: 28.05%) and O=C–O (from 288.77 eV: 38.37% to 288.83 eV: 44.16%), were detected for the PLA MPs after Cd(II) adsorption, indicating that the oxygen groups of the PLA MPs were closely associated with Cd(II) interactions. The variation of oxygen groups was also found in the PP MPs but much weaker (Fig. 4(b) and Table S4). Different changing trends were observed for the peaks in the PA MP spectrum. The C 1s peaks at 285.49 and 287.98 eV (Fig. 4(c)) were assigned to the C–N and O=C–N groups of the amides, respectively (Tang et al., 2022). Unlike the PLA MPs, the proportions of C–N and O=C–N increased for the PA MPs (Table S5), consistent with the changing trends of N 1s and O 1s (Table 3). Moreover, both the binding energy of C–N (from 285.49 to 285.36 eV) and O=C–N (from 287.98 to 287.77 eV) displayed shifts to lower energies, indicating that the amide groups (–CONH–) of PA MPs participated in the interactions with the Cd(II) ions (Zheng et al., 2021).

3.3.2 2D FTIR COS maps of MPs before and after Cd(II) adsorption

The main peak assignments in the FTIR spectra of the original PLA, PP, and PA samples before and after Cd(II) adsorption are presented in Table S6. No new peaks were identified, and only minor changes in the main peaks were observed in the FTIR spectra of the MPs examined before and after Cd(II) adsorption (Fig. S3). Since the information provided by one-dimensional FTIR spectra was too limited to interpret the roles of the different functional groups during Cd(II) adsorption, 2D FTIR COS analyses were performed. The 2D COS maps for the range 1800–900 cm^{-1} are presented in Fig. 5. Significant variations were detected in the 2D COS maps for the range 1800–900 cm^{-1}, which included the major bands corresponding to amides, esters, and aliphatic groups in the examined MPs (Li et al., 2019).

For the PLA MPs, five autopeaks were observed along the diagonal line of the synchronous 2D COS map (Fig. 5(a)), and these occurred at 1748, 1083, 1180, 1128, and 1040 cm^{-1} with the intensities decreasing in that

Table 3 Atomic percentages (%) from XPS analyses of the elements on the PLA, PP, and PA microplastics (MPs) before and after Cd(II) adsorption

MPs	Cd(II) adsorption	C 1s	O 1s	N 1s	Cd 3d [a)]	O/C	N/C [b)]
PLA	Before adsorption	61.83	37.62	0.53	0.02	0.61	–
	After adsorption	60.99	38.38	0.61	0.02	0.63	–
PP	Before adsorption	97.23	2.48	0.87	0.05	0.03	–
	After adsorption	94.60	4.59	0.78	0.03	0.05	–
PA	Before adsorption	77.47	15.01	7.49	0.03	0.19	0.10
	After adsorption	76.37	13.20	10.38	0.05	0.17	0.14

Notes: a) Cd atomic percentages for all three MPs were below 0.05%; b) – means N/C ratio was not over 0.01.

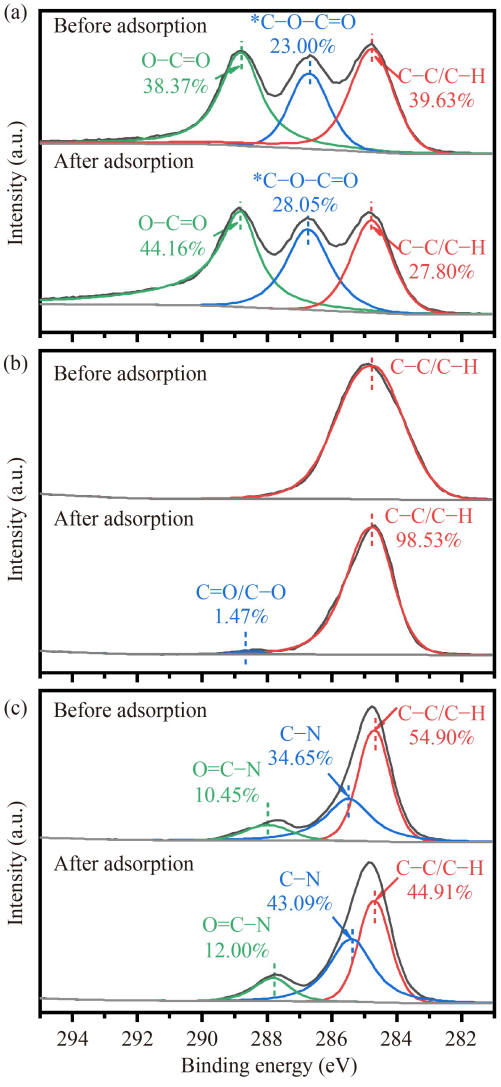

Fig. 4 XPS C 1s spectra of (a) PLA, (b) PP, and (c) PA microplastics (MPs) before and after Cd(II) adsorption.

order. The peaks at 1748, 1083, 1180, and 1128 cm^{-1} represented the stretching vibrations of the C=O, C–O, C–O–C and C–C bonds (Table S6), respectively. There was no overt autopeak found for the C–H bonds (e.g., 1454, 1383, 1358 cm^{-1}), indicating a more vital role of the oxygen groups during Cd(II) adsorption. All of the cross-peaks for the C=O, C–O, and C–O–C bonds showed positive signals, suggesting that these specific groups underwent synchronous variations. These variation trends coincided with the differences in the C=O and C–O proportions indicated by the XPS analyses of the PLA MPs (Table 4). According to Noda's rules (Noda and Ozaki, 2005), asynchronous 2D COS maps can reveal the variation order for specific chemical bonds. Three obvious cross-peaks ((1454, 1748 cm^{-1}), (1180, 1748 cm^{-1}), and (1083, 1748 cm^{-1})) presented negative signs in the asynchronous 2D COS map for the PLA MPs (Fig. 5(b)), and two positive cross-peaks ((1180, 1358 cm^{-1}) and (1083, 1358 cm^{-1})) were identified. As these five cross-peaks were positive in Fig. 5(a), these indicated that the variation order for the PLA MPs was as follows: C=O → C–O → C–H. In brief, these results demonstrated that the specific oxygen groups (C=O and C–O) of the PLA MPs combined with Cd(II) ions more effectively than the C–H and C–C groups during the adsorption process (Li et al., 2021).

In the synchronous 2D COS map for the PA MPs (Fig. 5(c)), two remarkable autopeaks were identified at 1632 and 1533 cm^{-1}, which represented the amide I (–**CO**–NH–) and amide II (–CO–**NH**–) bands, respectively. The cross-peak at 1632 and 1533 cm^{-1} showed positive signals, suggesting simultaneous changes in the C=O and N–H bonds. Moreover, the cross-peaks at (1533, 1632 cm^{-1}), (1463, 1632 cm^{-1}), and (1463, 1533 cm^{-1}) were positive in both the synchronous and asynchronous 2D COS maps for the PA MPs (Figs. 5(c) and 5(d)), which implied the sequential order C–H → C=O → N–H. However, only several peaks representing $–CH_2–$ and $–CH_3$ structures (e.g., 1455 and 1376 cm^{-1}) were found in the 2D COS maps for the PP MPs, as shown in Figs. 5(e) and 5(f).

3.4 Biodegradable PLA MPs *vs.* conventional nonbiodegradable MPs: Cd(II) adsorption characteristics and mechanisms

Different Cd(II) adsorption capacities were found for the biodegradable (PLA MPs) and nonbiodegradable MPs (PA and PP MPs) in the current study. The maximum Cd(II) adsorption capacities detected for the PA and PP

Table 4 C 1s and O 1s component peaks for the PLA microplastics (MPs) before and after Cd(II) adsorption

Core level	Assignment	Before Cd(II) adsorption			After Cd(II) adsorption		
		Binding energy (eV)	Area	Component percentage (%)	Binding energy (eV)	Area	Component percentage (%)
C 1s	C–C/C–H	284.77	68743	38.63	284.78	52128	27.80
	C–O–C=O	286.68	40873	23.00	286.73	52128	28.05
	O–C=O	288.77	68089	38.37	288.83	82591	44.16
O 1s	C=O	532.14	86304	33.27	532.10	154682	54.11
	C–O–H	533.49	143543	55.40	533.47	102958	36.05
	O=C–**O**	538.48	29248	11.33	537.69	27995	9.84

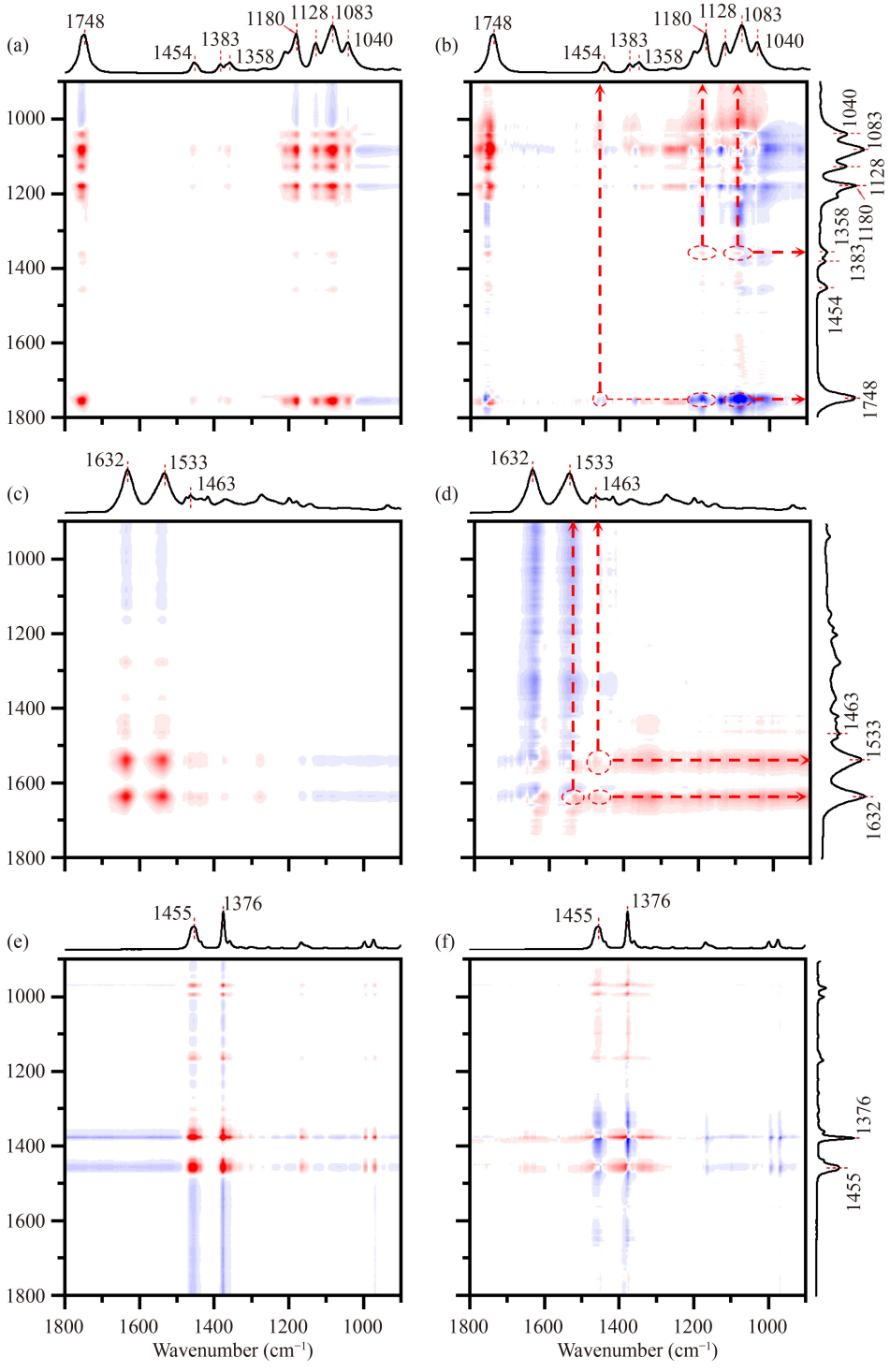

Fig. 5 2D FTIR COS maps for the microplastics (MPs): (a) synchronous and (b) asynchronous maps for the PLA MPs; (c) synchronous and (d) asynchronous maps for the PA MPs; (e) synchronous and (f) asynchronous maps for the PP MPs. The red and blue colors in the maps indicate positive and negative correlations, respectively.

MPs in our study were 0.96 ± 0.07 and 0.22 ± 0.03 mg/g, respectively, which were comparable to the results reported in previous literature (Table S7). The PLA MPs in our study showed a Cd(II) adsorption capacity of 0.64 ± 0.04 mg/g, which was higher than those of many conventional MPs examined in the literature (i.e., 0.0133–0.3610 mg/g for PP MPs and 0.0305–0.3663 mg/g for PE MPs, as presented in Table S7).

Physical characteristics, such as pore volume, specific surface area, and crystallinity, might be important factors influencing the Cd(II) adsorption processes of different MPs, as previously reported. For example, it has been

observed that MPs with higher specific surface area or lower crystallinity would have a greater adsorption capacity of heavy metals (Guo et al., 2020; Zhou et al., 2020). However, it is interesting to note that the PLA MPs showed a remarkably higher Cd(II) adsorption capacity than PP MPs (approximately 2.9 times) in our study, although the PLA MPs had a similar total pore volume and specific surface area, but a higher crystallinity than the PP MPs (Table S1). Moreover, the PA MPs had a lower specific surface area but higher Cd(II) adsorption capacity than the PLA MPs. Thus, these regularities about the physical characteristics reported in previous studies could not explain the differences among the MPs examined in our study.

The XPS and 2D FTIR COS analyses before and after Cd(II) adsorption demonstrated distinct changes in the surface chemical structures of the three examined MPs and revealed their major Cd(II) adsorption sites. For the PLA MPs, the C=O and C–O structures, rather than the C–H bonds, combined with the Cd(II) ions during the Cd(II) adsorption process. As the O atoms in the C=O and C–O groups can combine with divalent metal ions while serving as electron donors, surface complexation might dominate the binding process, leading to augmentation of the C=O/C–O groups (Tang et al., 2021). No obvious change was detected for the C–C/C–H groups in the PP MPs during the Cd(II) adsorption process, consistent with the conclusions of Guo et al. (2020), who noted that physical adsorption was likely to be the dominant mechanism. Thus, the different dominant adsorption mechanisms explained why the PLA MPs showed a remarkably higher adsorption capacity than the PP MPs. In addition, our XPS (Fig. 4(b)) and 2D FTIR COS results (Figs. 5(c) and 5(d)) indicated that N–H and C=O groups were the major binding sites for Cd(II) adsorption by the PA MPs, which was consistent with the results of Li et al. (2021). The N atoms of C–N/N–H and the O atoms of C=O can donate their lone pair electrons to metal ions (e.g., Cu^{2+}, Pb^{2+}, Cd^{2+}); hence, complexation contributed to the Cd(II) adsorption process (Tang et al., 2022). It could be speculated that the specific oxygen (and nitrogen) groups (i.e., Cd(II) adsorption sites) were the dominant causes of the different Cd(II) adsorption capacities observed for the PLA and PA MPs.

As the current study indicated that the specific oxygen groups led to the high adsorption capacity of biodegradable PLA MPs, it was noticed that other common biodegradable plastics, including polycaprolactone (PCL), polyhydroxyalkanoates (PHA), and polybutylene adipate terephthalate (PBAT), were typical polyester plastics possessing the same oxygen functional groups as PLA. Consequently, these biodegradable MPs deserve further investigations of their interactions with heavy metals, considering their potentially higher adsorption capacities and the greater environmental threats they might pose compared to conventional nonbiodegradable MPs.

3.5 Biodegradable PLA MPs *vs.* conventional nonbiodegradable MPs: Cd(II) desorption and bioaccessibility in the human gastrointestinal environment

In the control group (both Ctrl (1 h) and (5 h)), Cd(II) adsorbed on all of the examined MPs showed very low desorption capacities (0.024–0.039 mg/g) compared to their adsorption capacities (Fig. 6(a)). The Cd(II) desorption ratios (%) decreased in the order PP > PLA > PA MPs, which was opposite to the order for the adsorption capacities (PA > PLA > PP) obtained in adsorption experiments. Theoretically, the desorption ratio is associated with the binding force between the MPs and Cd(II) ions. Thus, the lower desorption ratios for the PLA and PA MPs could indicate stronger binding between oxygen (and nitrogen) groups and adsorbed Cd(II) ions, while the Cd(II) adsorbed on the PP MPs was easily exchanged by Na^+ in the Ctrl solution due to the weaker physical interactions (Zhang et al., 2020).

The Cd(II) desorption capacities of all three MPs were significantly enhanced in both the gastric and intestinal phases. This was consistent with previous studies showing that higher temperature, lower pH, and competitive adsorption of enzymes promoted the release of heavy metals from MPs, leading to high bioaccessibilities (Li et al., 2022). Interestingly, even though the PLA MPs neither exhibited the highest adsorption capacity nor were most able to release absorbed Cd(II) in the Ctrl group, the *in vitro* bioaccessibility of the Cd(II) on PLA MPs (19% in the gastric phase and 62% in the intestinal phase, as shown in Fig. 6(b)) was higher than those observed with the PA MPs (13% in the gastric phase and 22% in the intestinal phase) or PP MPs (18% in the gastric phase and 26% in the intestinal phase). As a type of biodegradable and biocompatible polyesters, the ester groups (–COO–) of PLA can be hydrolyzed *in vivo* by esterase and acid, as reported. For example, Landry et al. (1996) confirmed that PLA nanoparticles were degraded rapidly and then converted into lactate, mainly due to an enzymatic cleavage process. Wang et al. (2023) demonstrated that PLA MPs were degraded and generated nanoplastics and oligomers by competing for lipase during gastrointestinal processes.

To explore the physicochemical changes occurring in the PLA MPs, we determined the morphologies of the three MPs after the digestive process. In particular, many distinct pits and cracks were formed on the surfaces of the PLA MPs, as shown in Figs. 1(g) and 1(j), while the PP (Figs. 1(h) and 1(k)) and PA MPs (Figs. 1(i) and 1(l)) maintained their integrities in both the gastric and intestinal phases. In addition, the lactic acid concentrations of the filtered solutions were significantly higher after the intestinal phase (~1.9 mmol/L) compared to the Blank group without MPs (Fig. 6(c)). These results demonstrated degradation of the PLA MPs in the gastric and intestinal phases. Accordingly, enzymatic cleavage in

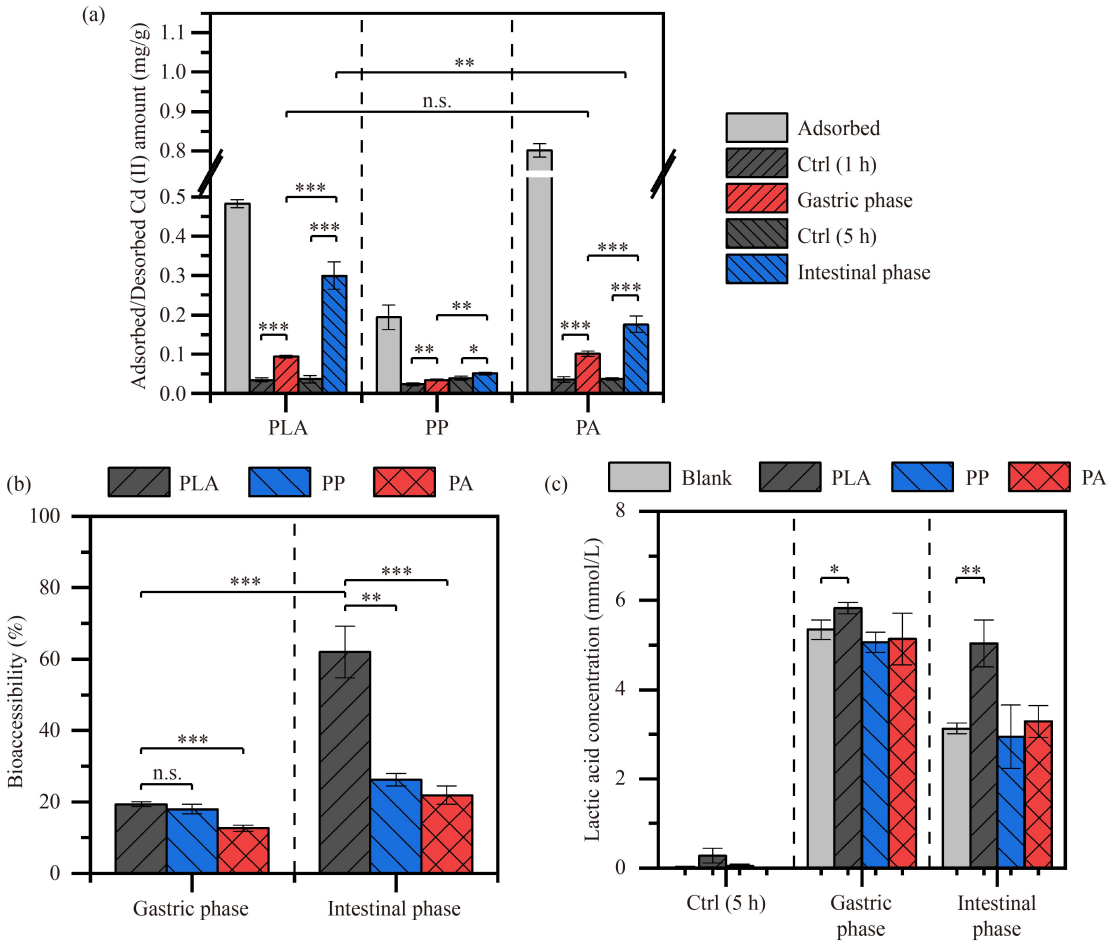

Fig. 6 *In vitro* assay results for PLA, PP, and PA microplastics (MPs) in the simulated gastric and intestinal phases: (a) adsorbed (initial) and desorbed Cd(II) amounts (mg/g); (b) bioaccessibility (%) of Cd(II) adsorbed on MPs; (c) lactic acid concentrations (mmol/L) of the filtered gastric and intestinal fluids. Statistically significant differences were determined with one-way ANOVA (n.s.: not significant; ***$P < 0.001$; **$P < 0.01$; *$P < 0.05$).

the gastrointestinal environment is likely to stimulate the release of Cd(II) ions by competing for the main binding sites, namely, the ester bonds of the PLA MPs. Additionally, due to the generation of lactic acid monomers and oligomers in the digestive fluids, the Cd(II) on the MPs could be transferred to the digestive fluids and become more bioaccessible in the human body. In summary, the high Cd(II) bioaccessibility of the PLA MPs was attributed to the degradation of biodegradable PLA during human digestion, which was not observed in the Cd(II) desorption processes of the PA and PP MPs.

Furthermore, one limitation of this study is that only the simulated gastrointestinal environment was investigated. In fact, the real gastrointestinal environment is much more complicated by other factors, such as microorganisms and the gastrointestinal motor, which might alter the degradation process (including hydrolytic, enzymatic, and microbial degradation) of the biodegradable MPs. Thus, further attention should be given to the physicochemical changes occurring in the biodegradable MPs during the human digestive process, which might alter gastrointestinal fates and toxicity for the MPs and co-contaminants that differ from those of conventional nonbiodegradable MPs.

4 Conclusions

This study was the first to determine the differences in Cd(II) adsorption and desorption characteristics and mechanisms for biodegradable PLA MPs and two conventional nonbiodegradable MPs (PP and PA). The main results are:

1) The maximum adsorption capacities detected for the MPs with batch adsorption experiments decreased in the order PA (0.96 ± 0.07 mg/g) > PLA (0.64 ± 0.04 mg/g) > PP (0.22 ± 0.03 mg/g). The adsorption behaviors of the PLA MPs were well described by the Pseudo-second-order and Freundlich models, as were those of the PA MPs but different from the PP MPs.

2) The specific oxygen groups in the PLA MPs served as the major and preferred binding sites for Cd(II) during

adsorption, so the PLA MPs exhibited a remarkable adsorption capacity. The dominant Cd(II) adsorption mechanism for the PLA and PA MPs was surface complexation, while there were only physical interactions between Cd(II) and the PP MPs.

3) The significant increase in soluble lactic acid as well as the cracks on the surfaces of PLA MPs indicated degradation of the PLA MPs during *in vitro* human digestion. Consequently, the Cd(II) on the biodegradable PLA MPs was more easily released during human digestion than that on the PP and PA MPs, resulting in higher bioaccessibility (19% in the gastric phase and 62% in the intestinal phase) and subsequent toxicity.

This work highlights the remarkable capability of biodegradable MPs to accumulate Cd(II) and release it to the human body. Notably, potential degradation of the biodegradable MPs during human digestion could make the adsorbed heavy metals more bioaccessible, which might make the biodegradable MPs a more severe health threat than conventional nonbiodegradable MPs.

Acknowledgements This study was financially supported by the Hubei Provincial Natural Science Foundation of China (Nos. 2021CF349 and 2020CFA042).

Declaration of Competing Interest The authors declare that they have no known competing financial interests or personal relationships that could have appeared to influence the work reported in this paper.

Electronic Supplementary Material Supplementary material is available in the online version of this article at https://doi.org/10.1007/s11783-024-1779-4 and is accessible for authorized users.

References

Dong Y, Gao M, Song Z, Qiu W (2019). Adsorption mechanism of As(III) on polytetrafluoroethylene particles of different size. Environmental Pollution, 254: 112950

Duan Z, Cheng H, Duan X, Zhang H, Wang Y, Gong Z, Zhang H, Sun H, Wang L (2022). Diet preference of zebrafish (*Danio rerio*) for bio-based polylactic acid microplastics and induced intestinal damage and microbiota dysbiosis. Journal of Hazardous Materials, 429: 128332

Guo X, Hu G, Fan X, Jia H (2020). Sorption properties of cadmium on microplastics: the common practice experiment and a two-dimensional correlation spectroscopic study. Ecotoxicology and Environmental Safety, 190: 110118

Haider T P, Volker C, Kramm J, Landfester K, Wurm F R (2019). Plastics of the future? The impact of biodegradable polymers on the environment and on society. Angewandte Chemie International Edition, 58(1): 50–62

Landry F B, Bazile D V, Spenlehauer G, Veillard M, Kreuter J (1996). Degradation of poly(*d*,*l*-lactic acid) nanoparticles coated with albumin in model digestive fluids (USP XXII). Biomaterials, 17(7): 715–723

Li C, Busquets R, Campos L C (2020). Assessment of microplastics in freshwater systems: a review. Science of the Total Environment, 707: 135578

Li W, Zu B, Yang Q, Huang Y, Li J (2022). Adsorption of lead and cadmium by microplastics and their desorption behavior as vectors in the gastrointestinal environment. Journal of Environmental Chemical Engineering, 10(3): 107379

Li X, Li M, Mei Q, Niu S, Wang X, Xu H, Dong B, Dai X, Zhou J L (2021). Aging microplastics in wastewater pipeline networks and treatment processes: physicochemical characteristics and Cd adsorption. Science of the Total Environment, 797: 148940

Li X, Mei Q, Chen L, Zhang H, Dong B, Dai X, He C, Zhou J (2019). Enhancement in adsorption potential of microplastics in sewage sludge for metal pollutants after the wastewater treatment process. Water Research, 157: 228–237

Liao Y L, Yang J Y (2020). Microplastic serves as a potential vector for Cr in an *in-vitro* human digestive model. Science of the Total Environment, 703: 134805

Liao Y L, Yang J Y (2022). The release process of Cd on microplastics in a ruminant digestion *in-vitro* method. Process Safety and Environmental Protection, 157: 266–272

Liu X, Wang J (2020). Algae (*Raphidocelis subcapitata*) mitigate combined toxicity of microplastic and lead on *Ceriodaphnia dubia*. Frontiers of Environmental Science & Engineering, 14(6): 97

Napper I E, Thompson R C (2019). Environmental deterioration of biodegradable, *oxo*-biodegradable, compostable, and conventional plastic carrier bags in the sea, soil, and open-air over a 3-year period. Environmental Science & Technology, 53(9): 4775–4783

Noda I, Ozaki Y (2005). Two-dimensional Correlation Spectroscopy: Applications in Vibrational and Optical Spectroscopy. Hoboken: John Wiley & Sons

Oliveri Conti G, Ferrante M, Banni M, Favara C, Nicolosi I, Cristaldi A, Fiore M, Zuccarello P (2020). Micro- and nano-plastics in edible fruit and vegetables: the first diet risks assessment for the general population. Environmental Research, 187: 109677

Plastics Europe (2021). Plastics—The facts: an Analysis of European Plastics Production, Demand and Waste Data. Brussels: Plastics Europe

Prata J C, Da Costa J P, Lopes I, Duarte A C, Rocha-Santos T (2020). Environmental exposure to microplastics: an overview on possible human health effects. Science of the Total Environment, 702: 134455

Qiu Y, Zheng M, Wang L, Zhao Q, Lou Y, Shi L, Qu L (2019). Sorption of polyhalogenated carbazoles (PHCs) to microplastics. Marine Pollution Bulletin, 146: 718–728

Ruby M V, Davis A, Schoof R, Eberle S, Sellstone C M (1996). Estimation of lead and arsenic bioavailability using a physiologically based extraction test. Environmental Science & Technology, 30(2): 422–430

Sarkar D J, Das Sarkar S, Das B K, Sahoo B K, Das A, Nag S K, Manna R K, Behera B K, Samanta S (2021). Occurrence, fate and removal of microplastics as heavy metal vector in natural wastewater treatment wetland system. Water Research, 192: 116853

Tang S, Lin L, Wang X, Feng A, Yu A (2020). Pb(II) uptake onto nylon microplastics: interaction mechanism and adsorption performance. Journal of Hazardous Materials, 386: 121960

Tang S, Lin L, Wang X, Yu A, Sun X (2021). Interfacial interactions

between collected nylon microplastics and three divalent metal ions (Cu(II), Ni(II), Zn(II)) in aqueous solutions. Journal of Hazardous Materials, 403: 123548

Tang S, Yang X, Zhang T, Qin Y, Cao C, Shi H, Zhao Y (2022). Adsorption mechanisms of metal ions (Pb, Cd, Cu) onto polyamide 6 microplastics: new insight into environmental risks in comparison with natural media in different water matrices. Gondwana Research, 110: 214–225

UNEP (2021). From Pollution to Solution: a Global Assessment of Marine Litter and Plastic Pollution. Nairobi: United Nations Environment Programme (UNEP)

Wang F, Yang W, Cheng P, Zhang S, Zhang S, Jiao W, Sun Y (2019). Adsorption characteristics of cadmium onto microplastics from aqueous solutions. Chemosphere, 235: 1073–1080

Wang M, Li Q, Shi C, Lv J, Xu Y, Yang J, Chua S L, Jia L, Chen H, Liu Q, et al. (2023). Oligomer nanoparticle release from polylactic acid plastics catalysed by gut enzymes triggers acute inflammation. Nature Nanotechnology, 18(4): 403–411

Wei X F, Bohlen M, Lindblad C, Hedenqvist M, Hakonen A (2021). Microplastics generated from a biodegradable plastic in freshwater and seawater. Water Research, 198: 117123

Yang J, Cang L, Sun Q, Dong G, Ata-Ul-Karim S T, Zhou D (2019). Effects of soil environmental factors and UV aging on Cu^{2+} adsorption on microplastics. Environmental Science and Pollution Research International, 26(22): 23027–23036

Yu Y, Ding Y, Zhou C, Ge S (2023). Aging of polylactic acid microplastics during hydrothermal treatment of sewage sludge and its effects on heavy metals adsorption. Environmental Research, 216(Pt 2): 114532

Zhang H, Wang J, Zhou B, Zhou Y, Dai Z, Zhou Q, Chriestie P, Luo Y (2018). Enhanced adsorption of oxytetracycline to weathered microplastic polystyrene: kinetics, isotherms and influencing factors. Environmental Pollution, 243(Pt B): 1550–1557

Zhang S, Han B, Sun Y, Wang F (2020). Microplastics influence the adsorption and desorption characteristics of Cd in an agricultural soil. Journal of Hazardous Materials, 388: 121775

Zheng Y, Rao F, Zhang M, Li J, Huang W (2021). Efficient, selective, and reusable metal–organic framework-based adsorbent for the removal of Pb(II) and Cr(VI) heavy-metal pollutants from wastewater. Cleaner Engineering and Technology, 5: 100344

Zhou Y, Yang Y, Liu G, He G, Liu W (2020). Adsorption mechanism of cadmium on microplastics and their desorption behavior in sediment and gut environments: the roles of water pH, lead ions, natural organic matter and phenanthrene. Water Research, 184: 116209